buildings

MDPI

Article

Fracture Mechanical Properties of Steel Fiber Reinforced Self-Compacting Concrete under Dry–Wet Cycle Sulfate Attack

Junxia Liu [1,2,*], Shujie Zang [1], Fei Yang [1,2,*], Maoliang Zhang [3] and Anbang Li [1]

[1] School of Architectural Engineering, Zhongyuan University of Technology, Zhengzhou 450007, China
[2] Henan Province Engineering Research Center of Green and High-Performance Cement-Based Composite Materials and Structures, Zhengzhou 450007, China
[3] Henan Building Materials Research and Design Institute Co., Ltd., Zhengzhou 450002, China
* Correspondence: liujunxia80600@163.com (J.L.); 15515572372@163.com (F.Y.); Tel.: +86-155-1557-2372 (F.Y.)

Abstract: Sulfate attack is the most common form of the durability damage of hydraulic concrete, and the performance degradation of cracked structural components is more significant at the position of water level change. Fly ash, a widely utilized supplementary cementitious material, can effectively improve the durability of concrete. In this paper, fly ash was used to partially replace Portland cement at 0 w%, 40 w%, 50 w%, 60 w%, and 70 w%, respectively. Through the three-point bending beam test with notch and the dry–wet cycle of sulfate attack, the change law of the fly ash content on the fracture mechanical properties of steel fiber reinforced self-compacting concrete (SFSCC) and its degradation mechanism under sulfate attack was studied. The results show that the load–crack mouth opening displacement curve of SFSCC changed from a steamed bread peak to a sharp peak under 30 dry–wet cycles of sulfate attack. The fracture toughness, peak load, and fracture energy of SFSCC with a high-volume fly ash increased with the increase in the fly ash content, while they reversed after sulfate attack. When the percentage of fly ash was 70 w%, the retention ratio of the fracture parameters was lower than that of SFSCC without incorporating fly ash, and when the percentage of fly ash was 50 w%, SFSCC had good bearing capacity, fracture mechanical properties, and corrosion resistance. The corrosion product of the reference SFSCC with 30 dry–wet cycles of sulfate attack was ettringite, whereas the SFSCC with a high-volume fly ash had no obvious corrosion products and the microstructure became looser.

Keywords: self-compacting concrete; fracture mechanical property; dry–wet circle; sulfate attack; fly ash; corrosion resistance

Citation: Liu, J.; Zang, S.; Yang, F.; Zhang, M.; Li, A. Fracture Mechanical Properties of Steel Fiber Reinforced Self-Compacting Concrete under Dry–Wet Cycle Sulfate Attack. *Buildings* **2022**, *12*, 1623. https://doi.org/10.3390/buildings12101623

Academic Editor: Ahmed Senouci

Received: 1 September 2022
Accepted: 5 October 2022
Published: 7 October 2022

1. Introduction

Sulfate attack is an extremely complex physical and chemical process [1,2], where its essence is that SO_4^{2-} reacts with hydration products to produce expansive erosion products, resulting in local stress concentration [3,4]. Sulfate attack can easily cause structural damage to buildings [5,6], and seriously affects its service life [7]. Hydraulic building components exposed to seawater, groundwater, or industrial wastewater with high concentrations of sulfate for a long time, especially concrete located in the water level fluctuation areas, splash areas, and tidal areas, will suffer from the combined effects of wet and dry cycles and sulfate attack, and the deterioration of concrete performance is more significant [8,9].

Some scholars have pointed out that mineral admixtures effectively improve the compactness, impermeability, and erosion resistance of concrete through the micro-aggregate effect and pozzolanic activity [10,11], among which the research and application of fly ash are the most extensive [12]. The results of Ji et al. [13] showed that the long-term performance of concrete such as dry shrinkage resistance, sulfate resistance, and frost resistance was significantly improved when the magnesium slag content reached a certain level. Yi et al. [14] found that the incorporation of fly ash, slag, and silica fume into ordinary Portland cement improved the seawater corrosion resistance of concrete. The test results

from Wang et al. [15] showed that slag effectively improved the resistance to the sulfate dry–wet cycle erosion of concrete. The research of Jin et al. [16] concluded that fly ash helped to inhibit sulfate ions from entering the concrete and enhanced its ability to resist sulfate attack. The results of Esquinas et al. [17] illustrated that fly ash effectively improved the acid resistance, saturated water absorption, and sulfate attack performance of concrete. Xie et al. [18] further confirmed that fly ash effectively reduced the drying shrinkage of self-compacting concrete (SCC), and its sulfuric acid resistance improved with the fly ash content. Similar results were also obtained in the study by Ghafoori et al. [19].

As a multiphase composite quasi-brittle material, concrete is prone to producing microcracks, and during construction, maintenance, and use, their growth and propagation accelerate the entry of corrosive ions and the deterioration mechanical properties of concrete [20]. The fracture mechanical properties of concrete are very sensitive to the shape and path of cracks [21], which can thoroughly reflect the damage and deterioration of concrete. In cracked components under a dry–wet cycle sulfate environment, the initial cracks induce and accelerate physical and chemical damage to sulfate crystallization [22]. Most of the research results have shown that adding an appropriate volume fraction of fibers into concrete improves the ductility of concrete, thereby, improving the fracture mechanical properties of concrete [23,24]. Fibers inhibit or slow down the expansion and connection of cracks in the concrete matrix through bridging, thereby improving the fracture mechanical properties of concrete [25], and the improvement effect of steel fibers is particularly prominent [26]. However, under the coupled action of dry–wetting cycles and sulfate attack, the bonding properties of the steel fibers and concrete matrix change, and the degradation mechanism of the fracture mechanical properties of steel fiber reinforced concrete needs to be further studied.

The composition of SCC has the characteristics of a low water–cement ratio, large sand ratio, and a large dosage of cementitious materials and additives, which make the influencing factors of sulfate attack performance quite complex [27,28]. Benefiting from the advantages of high fluidity, uniformity, and stability, SCC is widely used in subsea tunnels, sea crossing bridges, ports and wharves, and other projects [29]. SCC is susceptible to sulfate attack due to its own characteristics, especially where the water level changes frequently, and concrete structural damage is much more serious than sustained immersion. The sulfate solution intrudes into the concrete through the cracks of the concrete itself and reacts with the concrete, which seriously degrades the fracture performance of the concrete, and then affects the service performance and life of the concrete structure.

Although many scholars have focused on the mechanical performance of concrete under dry–wet cycle sulfate attack and explored its degradation mechanism through experimental methods, the systematic study of SCC with high-content fly ash is still limited, especially regarding its fracture mechanical properties. Based on the previous research results of our research group on the workability and 28 d mechanical properties of SFSCC [30], SCC with a volume fraction of 0.75% steel fiber was used as the conference concrete. Through the three-point bending beam with notches and the dry–wet cycle sulfate attack test, this paper studied the change law of the fracture mechanical properties of SFSCC before and after erosion with fly ash content. Combined with SEM analysis, the attack mechanism of SCC was clarified. This study will also provide basic data supporting the durability evaluation of SCC and high-content fly ash SCC.

2. Materials and Methods

2.1. Materials

The chemical composition and performance parameters of ordinary Portland cement (P.O 42.5) and fly ash are listed in Tables 1 and 2. The specific surface area and activity index of the fly ash was 463 m^2/kg and 0.92, respectively. The slaked lime was industrial grade, and its CaO content was no less than 70 w%. Local river sand with a fineness modulus of 2.8 and nature gravel with a particle size ranging from 5 to 19 mm were used as the fine aggregate and the coarse aggregate, respectively. The steel fibers had a length of

35 ± 3 mm, thus having an aspect ratio of 63. The modulus and tensile strength of elasticity of steel fibers were 230 GPa and ≥ 380 MPa, respectively. The water reducing agent was a powdered polycarboxylate superplasticizer with a water reducing rate of 30%.

Table 1. The performance index of the ordinary Portland cement.

Setting Time (min)		Compressive Strength (MPa)		Flexural Strength (MPa)	
Initial	**Final**	**3 d**	**28 d**	**3 d**	**28 d**
240	321	27.2	52.3	5.6	8.6

Table 2. The chemical composition of the ordinary Portland cement and fly ash.

Composition	SiO_2	Al_2O_3	Fe_2O_3	CaO	MgO	SO_3	K_2O	Na_2O	Loss
Cement (w%)	17.43	5.23	3.54	60.87	3.15	3.43	1.04	0.35	4.96
Fly ash (w%)	55.84	26.38	5.04	3.97	2.01	0.32	1.24	0.26	4.94

2.2. Mixture Ratio and Physical and Mechanical Properties of SFSCC

The proportions of the SFSCC mixture are listed in Table 3. The total amount of fly ash and slaked lime powder of SFSCC-0, SFSCC-40, SFSCC-50, SFSCC-60, and SFSCC-70 accounted for 0, 40 w%, 50 w%, 60 w%, and 70 w% of the total amount of cementitious materials, respectively. The mass ratio of the fly ash and slaked lime powder was determined by the mortar strength of the cementitious materials referred to in the "Cement-Test Methods-Determination of Strength" (ISO 679-2009).

Table 3. The mix proportion of SFSCC.

Code	Cementitious Materials (kg/m^3)			W/B	Sand Proportion	Steel Fiber (v%)	Water Reducer (%)
	Cement	Fly Ash	Slaked Lime				
SFSCC-0	479.0	0	0	0.35	0.50	0.75	0.3
SFSCC-40	287.5	175.0	16.5	0.35	0.50	0.75	0.3
SFSCC-50	237.5	208.0	33.5	0.35	0.50	0.75	0.4
SFSCC-60	191.6	241.6	45.8	0.35	0.50	0.75	0.4
SFSCC-70	141.5	275.0	62.5	0.35	0.50	0.75	0.5

To ensure the uniform mixing of SFSCC, the mixing process was as follows: (1) All raw materials were weighed according to Table 3; (2) sand, gravel, cement, fly ash, and slaked lime were poured into the concrete mixer and dry stirred for 30 s; (3) half of the water and water reducing agent aqueous solution was added and mixed for 90 s; (4) half of the water and water reducing agent aqueous solution was added and stirred for 30 s; (5) during the stirring process, the steel fibers were sprinkled in several times, so that the steel fibers and the concrete mixture were evenly mixed; and (6) after the steel fibers were completely sprinkled into the fresh concrete, it was mixed for 180 s, and then the mixer was turned off.

The workability and mechanical properties at 28 days and 1 year of SCC were evaluated according to the "Technical Specification for Application of Self-compacting Concrete" (JGJ/T 283-2012) [31]. The test results are listed in Table 4, among which T_{500} was used to describe the extending speed of the SCC mixture, which was the time required for the fresh concrete from the beginning of lifting the slump cylinder to extend to a diameter of 500 mm, accurate to 0.1 s. Considering the manufacturing error of the test piece and the discreteness of the test results, three test blocks were taken from each group.

Table 4. The physical mechanical properties of SFSCC.

Code	Slump Flow (mm)	T_{500} (s)	J-Ring Flow (mm)	Compressive Strength (MPa)		
				28 d	1 Year	Attacked
SFSCC-0	600	6.1	560	51.1	91.1	88.3
SFSCC-40	590	8.2	575	59.5	94.5	96.4
SFSCC-50	585	9.2	550	60.2	99.1	95.1
SFSCC-60	595	10.4	560	47.3	84.7	76.2
SFSCC-70	590	7.9	540	41.6	72.6	61.7

2.3. Three-Point Bending Test

The three-point bending beam test with notches was conducted according to the relevant provisions of the RILEM test standard. The size of the three-point bending beam was 100 mm × 100 mm × 515 mm, the reserved crack height a_0 in the mid-span of the specimen was 40 mm, the crack width was 3 mm, and the span was S = 400 mm. Considering the manufacturing error of the test piece and the discreteness of the test results, three test blocks were taken from each group, and the median value was used for discussion in the experimental results and discussion in this paper. The schematic diagram of the size of the test piece and the loading method is presented in Figure 1. The test was carried out on a CDT1504 microcomputer servo hydraulic testing machine (as shown in Figure 2). The knife-edge steel sheets were pasted on both sides of the prefabricated crack of the specimen to fix the YYJ-4/10 clip-type extensometer to measure the opening displacement of the crack. During the test, displacement was used to control the loading, and the loading rate was 0.05 mm/min. The mid-span load–displacement curve (F–δ curve) and the crack opening displacement were collected by the displacement acquisition system and the clip-on extensometer built in the testing machine, respectively. Based on the collected load (F) and opening displacement (CMOD) values, the F–CMOD curve can be drawn.

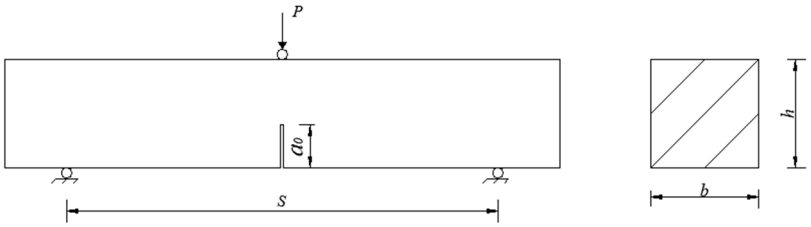

Figure 1. The specimen size and loading mode.

Figure 2. The three-point bending test process.

2.4. Dry–Wet Circle Sulfate Attack

For the dry–wet cycle sulfate attack test of SFSCC with high-volume fly ash, we referred to the "Standard for Long-term Performance and Durability Test of Ordinary Concrete" (GB/T50082-2009) [32]. The size of the specimen was the same as that of the three-point bending test.

It took 24 h to complete a cycle. The experimental process was as follows:

(1) The SCC specimens were soaked in 5 w% Na_2SO_4 solution for 15 h, as shown in Figure 3.
(2) The specimens were air-dried for 1 h, and then placed in an electric blast drying oven at 60 °C for 6 h, as shown in Figure 4.
(3) The specimens were cooled at room temperature for 2 h.

Figure 3. The specimens soaking in sodium sulfate solution.

Figure 4. The specimens drying in the oven.

2.5. SEM Analysis of SFSCC Section

The specimens for the scanning electron microscopy (SEM) adopted the edge part of the sample after the three-point bending test of the standard curing for 1 year, which were broken into 3–5 mm thin sheets with a regular shape, and then soaked in absolute ethanol for 24 h to stop hydration. The specimens were dried to a constant weight in a vacuum drying oven at 60 °C, and then sprayed with gold. The SCC specimens before and after sulfate attack were prepared in the same way. A Japanese JSM-7800F SEM was used to observe the microscopic morphology of the hydration and erosion products of SCC under the conditions of an accelerating voltage of 20 kV and a spot size of 3.

3. Experimental Results and Discussion

3.1. F–CMOD Curve Characteristics

It can be seen from Figure 5a that the F–CMOD curve of SFSCC curing for 1 year had an obvious quasi-elastic stage, stable crack growth stage and crack instability failure stage. Due to the enhanced crack resistance of the steel fiber, the F–CMOD curve of SFSCC was quite plump in the second and third stages, and still had considerable bearing and deformation capacity in the crack instability failure stage [33]. Figure 5b shows that the F–CMOD curves of SFSCC after 30 dry–wet cycles of sulfate attack changed from a steamed bread peak to a sharp peak. Specifically, the stable growth stage was evidently shortened, and the deformation of the SFSCC was reduced. It is noteworthy that the load reduction rate of the F–CMOD curves was higher than that of the corresponding original specimens in the crack instability failure stage. The results indicate that the fracture mechanical properties of SFSCC were degraded after 30 dry–wet cycles of sulfate attack.

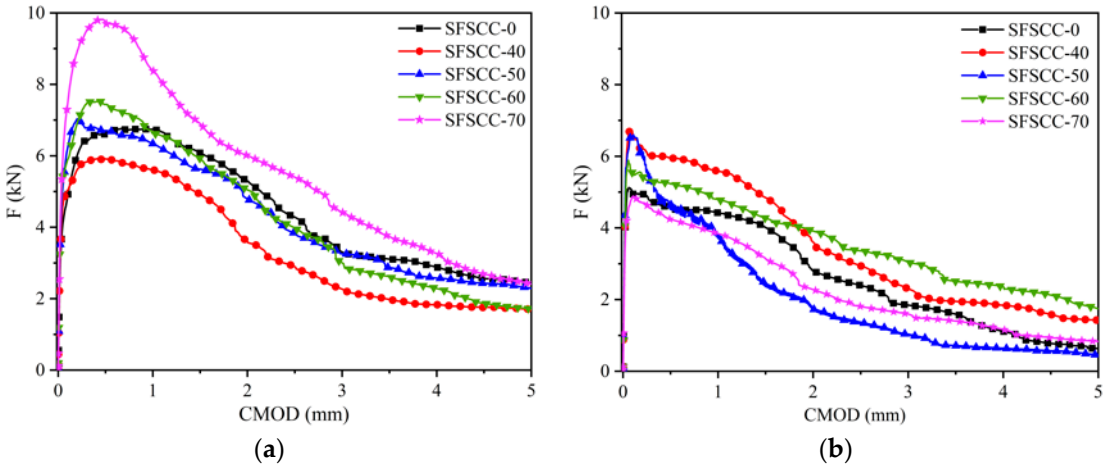

Figure 5. F–CMOD curve of SFSCC before and after dry–wet cycle sulfate attack. (**a**) Original SFSCC. (**b**) Sulfate attacked SFSCC.

3.2. Fracture Toughness and Peak Load

The fracture toughness (K_{IC}) of SCC was calculated by the F–CMOD curve obtained from the three-point bending beam test with the notch, as shown in Figure 5, and based on the fracture toughness Formula (1) given by the ASTM [34].

$$K_{IC} = \frac{F_{max}S}{bh^{3/2}} f(a/h) \quad (1)$$

$$f(a/h) = 2.9(a/h)^{1/2} - 4.6(a/h)^{3/2} + 21.8(a/h)^{5/2} - 37.6(a/h)^{7/2} + 38.7(a/h)^{9/2} \quad (2)$$

where F_{max} refers to the maximum load of three-point bending test (kN); S refers to the span length of the notched beam (mm); b and h refer to the width and height of notched beam (mm); a is the length of the effective crack (mm), calculated from the geometric relationship [35].

The K_{IC} and peak load (F_{peak}) of SFSCC before and after the dry–wet cycle sulfate attack are shown in Figure 6a,b, respectively.

Figure 6 shows that the fracture toughness (K_{IC}) and peak load (F_{peak}) of SFSCC with a high-volume fly ash increased with the fly ash content, while the K_{IC} and F_{peak} of the sulfate attacked SFSCC were opposite to those of the original. The K_{IC} and F_{peak} of SFSCC-40 were the lowest of all, and those of SFSCC-70 reached the maxima, which were 46% and 21% higher than SFSCC-0. It can be seen from Tables 3 and 4 that the relative content of slaked lime powder in the cementitious material increased with the fly ash content, which indicates that when cement is largely replaced by fly ash, the potential activity of fly ash can be effectively stimulated only when the cementitious material system maintains high

alkalinity [36]. The residual $Ca(OH)_2$ (CH) accordingly increases with the fly ash content after secondary hydration. A large number of hexagonal plate-like CH are tightly packed together with three-dimensional disorder in the hardened structure with low W/B and high density [37]. The slip between CH crystals helps to improve the deformation performance and tensile stress of SFSCC [38], so the K_{IC} and F_{peak} are correspondingly improved.

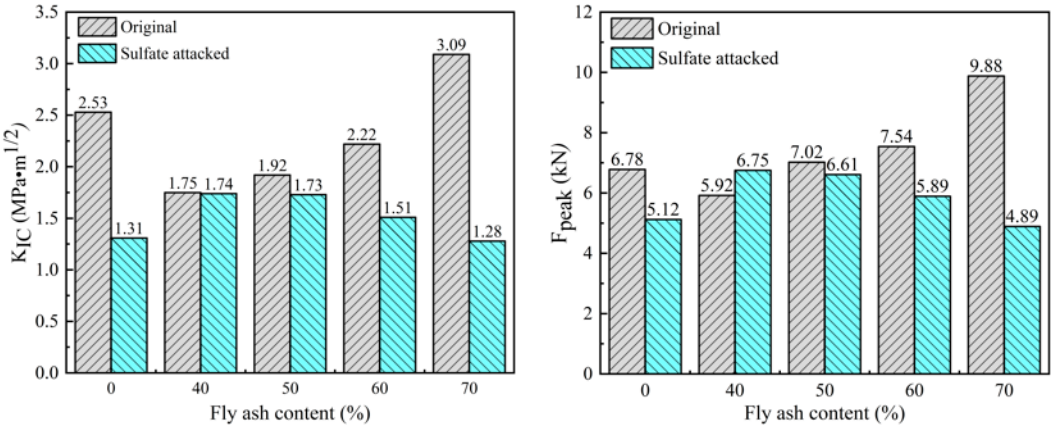

Figure 6. Fracture toughness and of SFSCC before and after dry–wet cycle sulfate attack. (**a**) Fracture toughness. (**b**) Peak load.

Figure 6 shows that the fracture toughness (K_{IC}) and peak load (F_{peak}) of SFSCC with a high-volume fly ash increased with the fly ash content, while the K_{IC} and F_{peak} of the sulfate attacked SFSCC were opposite to those of the original. The K_{IC} and F_{peak} of SFSCC-40 were the lowest of all, and those of SFSCC-70 reached the maxima, which were 46% and 21% higher than SFSCC-0. It can be seen from Tables 3 and 4 that the relative content of slaked lime powder in the cementitious material increased with the fly ash content, which indicates that when cement is largely replaced by fly ash, the potential activity of fly ash can be effectively stimulated only when the cementitious material system maintains high alkalinity [36]. The residual $Ca(OH)_2$ (CH) accordingly increases with the fly ash content after secondary hydration. A large number of hexagonal plate-like CH are tightly packed together with three-dimensional disorder in the hardened structure with low W/B and high density [37]. The slip between CH crystals helps to improve the deformation performance and tensile stress of SFSCC [38], so the K_{IC} and F_{peak} are correspondingly improved.

The K_{IC} and F_{peak} of sulfate attacked SFSCC-40 reached the maximum, and were not lower than those of the original SFSCC, and even the F_{peak} was 14% higher. The K_{IC} and F_{peak} of high-volume fly ash SFSCC decreased linearly with the continued increase in the fly ash content, but were still greater than SFSCC-0 when the dosage was not higher than 60%. The results indicate that the appropriate content of fly ash can ensure the fracture mechanical properties of the attacked SFSCC.

3.3. Fracture Energy

The fracture energy of concrete is the energy absorbed per unit area of crack propagation. According to the test results of the load (F) and mid-span displacement (δ) measured by the notched three-point bending beam test, the F–δ curve is drawn and calculated according to Formula (3), given by RILEM TC-50 [39].

$$G_F = \frac{W_0 + mg\delta_0}{b(h - a_0)} \quad (3)$$

where G_F refers to the fracture energy; W_0 refers to the area under the F–δ curve (N·m); m refers to the weight of the specimen between brackets (kg); g refers to the gravity constant (N/kg); δ_0 refers to the deflection at breakage (mm); a_0 refers to the notch depth (mm).

It can be seen from Table 5 that the variational law of G_F with the fly ash content was close to that of K_{IC} and F_{peak} before and after the dry–wet cycle sulfate attack. The G_F of the original SFSCC first decreased and then increased with the increase in the fly ash content, and SFSCC-40 was the lowest of all. The G_F of the sulfate attacked SFSCC first increased and then decreased with the fly ash content, with SFSCC-40 being the highest of them all. The G_F of the sulfate attacked SFSCC was significantly lower than that of the original, except for SFSCC-40, which indicates that the appropriate content of fly ash can improve the sulfate attack resistance of SFSCC, and enhance the bearing capacity and energy absorption capacity of in-service damaged components under a harsh environment [40,41]. According to Formula (3), when others parameter are close, the G_F is proportional to W_0, and W_0 is mainly determined by the F_{peak}, midspan displacement and the fullness of the F–δ curve. Since the above parameters of SFSCC are reduced to varying degrees after attack, the G_F is reduced accordingly.

Table 5. The fracture energy of SFSCC before and after sulfate attack.

Code	W_0 (N·m)		M (kg)		G_F (N/m)	
	Original	Attacked	Original	Attacked	Original	Attacked
SFSCC	20.97	12.34	9.75	9.68	3575	2136
SFSCC40	16.32	16.22	9.97	9.93	2801	2784
SFSCC50	20.55	12.63	9.80	9.75	3505	2185
SFSCC60	21.67	12.99	9.93	9.89	3693	2246
SFSCC70	30.09	10.79	9.92	9.90	5096	1879

3.4. Retention Ratio of Fracture Parameters

The retention ratio of mechanical properties is the ratio of the corresponding values of the original and the sulfate attacked specimens, which is often used to describe the corrosion resistance of concrete. This paper used it as the reference to describe the influence of 30 dry–wet cycles of sulfate attacks on the fracture parameters of SFSCC. It can be seen from Figure 7 that the retention ratio of the fracture parameters was significantly higher than that of SFSCC-0 when the fly ash content was 40 and 50%. The retention ratio of SFSCC-60 was slightly higher than that of SFSCC-0. The retention ratio of SFSCC-70 was significantly lower than that of SFSCC-0. The results indicate that the appropriate fly ash content can significantly improve the corrosion resistance of SCC [42], while the excessive content will obviously deteriorate.

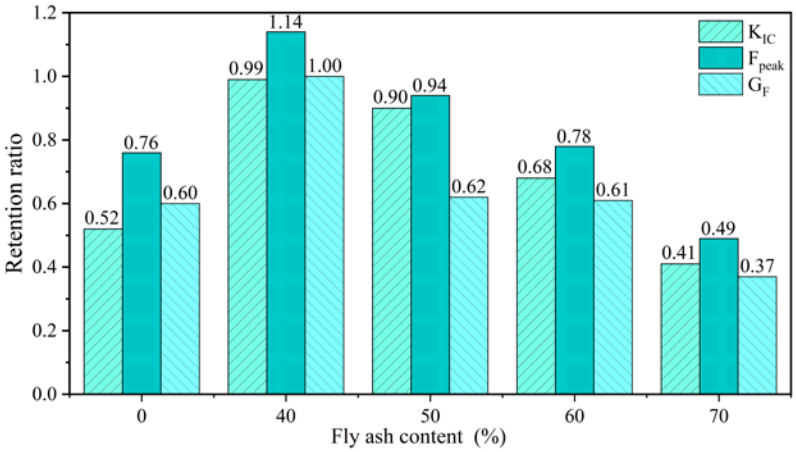

Figure 7. The fracture parameter retention ratio of SFSCC.

According to Tables 4 and 5 and Figures 5–7, the compressive strength and fracture parameters of the original SFSCC-50, except for K_{IC}, were close to those of SFSCC-0, and the retention ratio of the fracture parameters was higher than SFSCC-0. In other words,

when the content of fly ash was 50%, SFSCC had good bearing capacity, fracture mechanical properties, and corrosion resistance.

3.5. Microstructure of SFSCC before and after the Dry–Wet Cycle of Sulfate Attack

It can be seen from Figure 8a that the hardened structure of the benchmark SFSCC-0 was dense, the hydration product had a complete structure and crystallization, and there was a fibrous C–S–H gel between the interfaces. Figure 8b shows that the hydration products become fine, and a few hexagonal plate-shaped CH stacking was observed. Figure 8c,d are the microstructures of SFSCC-50 and SFSCC-60, respectively, and the layered stacking CH crystals, fly ash microbeads embedded in hydration products, pores, and micro-cracks can be seen from them.

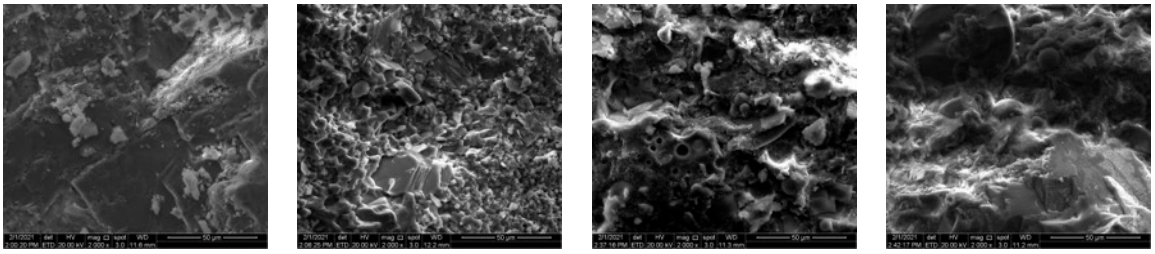

(**a**) (**b**) (**c**) (**d**)

Figure 8. Section SEM images of SFSCC at 1 year. (**a**) SFSCC-0 (2000×); (**b**)SFSCC-40 (2000×); (**c**) SFSCC-50 (2000×); (**d**) SFSCC-60 (2000×).

It can be seen from Figure 9a that the sulfate attacked products of SFSCC-0 was fascicled acicular ettringite, and its structure was loose. The local expansion caused by the formation of ettringite led to the reduction in its fracture mechanical properties. Figure 9b shows the section of SFSCC-40 after dry–wet cycle attack, where there was some fly ash particles and fine cracks, but no obvious corrosion products, and the hardened structure matrix was dense. Figure 9c,d shows that the microstructures of SFSCC-50 and SFSCC-60 were loose after erosion, that white erosion products appeared at the interface of the hydration products, and the microcracks and porosity increased. No obvious erosion products were observed in Figure 9c,d, and the cross-sectional structure of SFSCC-60 became looser.

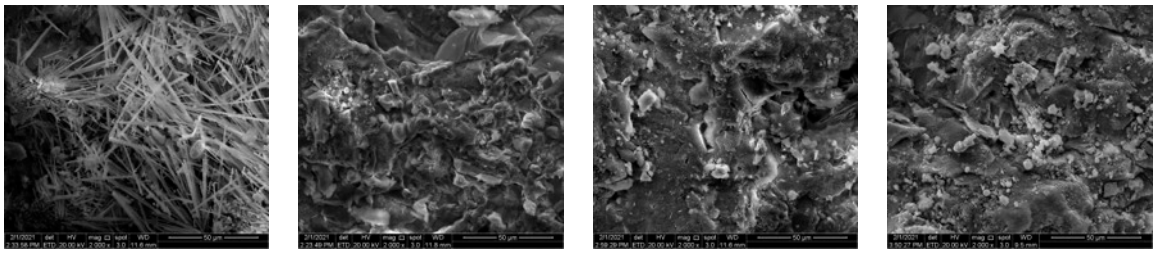

(**a**) (**b**) (**c**) (**d**)

Figure 9. Section SEM images of SFSCC under 30 dry–wet cycles of sulfate attack. (**a**) SFSCC-0 (2000×); (**b**) SFSCC-40 (2000×); (**c**) SFSCC-50 (2000×); (**d**) SFSCC-60 (2000×).

When the fly ash content was higher than 60%, the retention ratios of the fracture parameters were close to SFSCC-0, but significantly lower than SFSCC-40. This is due to the fact that the residual CH after secondary hydration increased with the fly ash content (Figure 8d). The residual CH increased the local stress concentration caused by the crystallization and expansion of ettringite and dihydrate gypsum. At the same time, during the drying and air cooling of the dry–wet cycles, the concentration of CH in the pore solution increased, and then carbonation occurred to produce $CaCO_3$. During

the subsequent process of sulfate attack, the C–S–H gel decomposed to produce non-cementitious thaumasite [43]. To sum up, an appropriate fly ash content in SFSCC can effectively improve its durability.

4. Conclusions

An experimental investigation was performed on the fracture mechanical properties of five groups of SFSCC under dry–wet cyclic sulfate attack. The degradation law and mechanism of the fracture parameters of SFSCC with a high-volume fly ash were studied. The results show that fly ash in an appropriate replacement content can effectively improve the fracture parameters and its retention ratios of SFSCC.

(1) The F–CMOD curve of SFSCC changed from a steamed bread peak to a sharp peak under 30 dry–wet cycles of sulfate attack. The K_{IC}, F_{peak}, and G_F of SFSCC increased with the increase in the fly ash content, and those of SFSCC-70 were the highest of all, which were 46%, 21%, and 43% higher than the benchmark SFSCC-0, respectively. The fracture parameters of the attacked SFSCC decreased with an increase in the fly ash content, K_{IC}, F_{peak}, and G_F of SFSCC-40 all reached a peak and increased by 33%, 32%, and 30% compared with SFSCC-0, respectively.

(2) When the contents of fly ash were 40 w%, 50 w%, and 60 w%, the retention ratio of the fracture parameters was higher than that of SFSCC-0. The compressive strength, fracture parameters, and retention ratio of SFSCC-50 were higher or close to those of SFSCC-0, in other words, when the content of fly ash was 50%, SFSCC had good bearing capacity, fracture mechanical properties, and corrosion resistance.

(3) The hardened structure of SFSCC-0 and SFSCC-40 was dense, and the hydration products of SFSCC-40 were finer than SFSCC-0. The microstructures of SFSCC-50 and SFSCC-60 were composed of the layered stacking CH crystals, fly ash microbeads, pores, and micro-cracks. The corrosion product of SFSCC-0 with 30 dry-wet cycles of sulfate attack was ettringite, and its damage was caused by local expansion, but SFSCC-40 had no obvious corrosion products. The white corrosion products at the interface of the hydration products were observed in the cross-sections of SFSCC-50 and SFSCC-60, and the microstructure of SFSCC-60 became looser.

Author Contributions: Conceptualization, J.L.; Methodology, F.Y.; Investigation, M.Z. and A.L.; Data curation, S.Z.; Writing-original draft preparation, S.Z. and J.L.; Writing-review and editing, F.Y. All authors have read and agreed to the published version of the manuscript.

Funding: This work was supported by the Independent Innovation Application Research Project of Zhongyuan University of Technology (No. K2020YY013).

Institutional Review Board Statement: Not applicable.

Informed Consent Statement: Not applicable.

Data Availability Statement: The data presented in this study are available in the article.

Conflicts of Interest: The authors declare no conflict of interest.

References

1. Cefis, N.; Comi, C. Chemo-mechanical modelling of the external sulfate attack in concrete. *Cem. Concr. Res.* **2017**, *93*, 57–70. [CrossRef]
2. Najjar, M.F.; Nehdi, M.L.; Soliman, A.M.; Azabi, T.M. Damage mechanisms of two-stage concrete exposed to chemical and physical sulfate attack. *Constr. Build. Mater.* **2017**, *137*, 141–152. [CrossRef]
3. Scherer, G.W. Stress from crystallization of salt. *Cem. Concr. Res.* **2004**, *34*, 1613–1624. [CrossRef]
4. Novak, G.A.; Colville, A.A. Efflorescent mineral assemblages associated with cracked and degraded residential concrete foundations in Southern California. *Cem. Concr. Res.* **1989**, *19*, 1–6. [CrossRef]
5. Ikumi, T.; Segura, I. Numerical assessment of external sulfate attack in concrete structures: A review. *Cem. Concr. Res.* **2019**, *121*, 91–105. [CrossRef]
6. Elahi, M.M.A.; Shearer, C.R.; Reza, A.N.R.; Saha, A.K.; Khan, M.N.N.; Hossain, M.M.; Sarker, P.K. Improving the sulfate attack resistance of concrete by using supplementary cementitious materials (SCMs): A review. *Constr. Build. Mater.* **2021**, *281*, 122628. [CrossRef]

7. Prithiviraj, C.; Swaminathan, P.; Kumar, D.R.; Murali, G.; Vatin, N.I. Fresh and Hardened Properties of Self-Compacting Concrete Comprising a Copper Slag. *Buildings* **2022**, *12*, 965. [CrossRef]
8. Gao, J.; Yu, Z.; Song, L.; Wang, T.; Wei, S. Durability of concrete exposed to sulfate attack under flexural loading and drying-wetting cycles. *Constr. Build. Mater.* **2013**, *39*, 33–38. [CrossRef]
9. Jiang, L.; Niu, D. Study of deterioration of concrete exposed to different types of sulfate solutions under drying-wetting cycles. *Constr. Build. Mater.* **2016**, *17*, 88–89. [CrossRef]
10. Li, Y.; Wang, R.; Li, S.; Zhao, Y.; Qin, Y. Resistance of recycled aggregate concrete containing low- and high-volume fly ash against the combined action of freeze-thaw cycles and sulfate attack. *Constr. Build. Mater.* **2018**, *166*, 23–34. [CrossRef]
11. Wang, D.; Zhou, X.; Meng, Y.; Chen, Z. Durability of concrete containing fly ash and silica fume against combined freezing-thawing and sulfate attack. *Constr. Build. Mater.* **2017**, *147*, 398–406. [CrossRef]
12. Jain, A.; Choudhary, S.; Gupta, R.; Chaudhary, S.; Gautam, L. Effect of granite industry waste addition on durability properties of fly ash blended self-compacting concrete. *Constr. Build. Mater.* **2022**, *340*, 127727. [CrossRef]
13. Ji, G.; Peng, X.; Wang, W.; Hu, C.; Ran, P.; Sun, K.; Zeng, L. Influence of magnesium slag as a mineral admixture on the performance of concrete. *Constr. Build. Mater.* **2021**, *295*, 123619. [CrossRef]
14. Yi, Y.; Zhu, D.; Guo, S.; Zhang, Z.; Shi, C. A review on the deterioration and approaches to enhance the durability of concrete in the marine environment. *Cem. Concr. Compos.* **2020**, *113*, 103695. [CrossRef]
15. Wang, D.; Ma, Y.; Kang, M.; Ju, Y.; Zeng, C. Durability of reactive powder concrete containing mineral admixtures in seawater erosion environment. *Constr. Build. Mater.* **2021**, *306*, 124863. [CrossRef]
16. Jin, Z.; Sun, W.; Zhang, Y.; Jiang, J.; Lai, J. Interaction between sulfate and chloride solution attack of concretes with and without fly ash. *Cem. Concr. Res.* **2007**, *37*, 1223–1232. [CrossRef]
17. Esquinas, A.R.; Álvarez, J.I.; Jiménez, J.R.; Fernández, J.M. Durability of self-compacting concrete made from non-conforming fly ash from coal-fired power plants. *Constr. Build. Mater.* **2018**, *189*, 993–1006. [CrossRef]
18. Xie, Y.; Liu, B.; Yin, J.; Zhou, S. Optimum mix parameters of high-strength self-compacting concrete with ultrapulverized fly ash. *Cem. Concr. Res.* **2002**, *32*, 477–480. [CrossRef]
19. Ghafoori, N.; Najimi, M.; Diawara, H.; Islam, M.S. Effects of class F fly ash on sulfate resistance of Type V Portland cement concretes under continuous and interrupted sulfate exposures. *Constr. Build. Mater.* **2015**, *78*, 85–91. [CrossRef]
20. Yin, Y.Y.; Hu, S.; Lian, J.; Liu, R. Fracture properties of concrete exposed to different sulfate solutions under drying-wetting cycles. *Eng. Fract. Mech.* **2022**, *266*, 108406. [CrossRef]
21. Sucharda, O.; Pajak, M.; Ponikiewski, T.; Konecny, P. Identification of mechanical and fracture properties of self-compacting concrete beams with different types of steel fibres using inverse analysis. *Constr. Build. Mater.* **2017**, *138*, 263–275. [CrossRef]
22. Kalousek, G.L.; Porter, L.C.; Benton, E.J. Concrete for long-time service in sulfate environment. *Cem. Concr. Res.* **1972**, *2*, 79–89. [CrossRef]
23. Kazemi, M.T.; Golsorkhtabar, H.; Beygi, M.H.A.; Gholamitabar, M. Fracture properties of steel fiber reinforced high strength concrete using work of fracture and size effect methods. *Constr. Build. Mater.* **2017**, *142*, 482–489. [CrossRef]
24. Yoo, D.Y.; Yoon, Y.S.; Banthia, N. Predicting the post-cracking behavior of normal-and high-strength steel-fiber-reinforced concrete beams. *Constr. Build. Mater.* **2015**, *93*, 477–485. [CrossRef]
25. Kurihara, N.; Kunieda, M.; Kamada, T.; Uchida, Y.; Rokugo, K. Tension softening diagrams and evaluation of properties of steel fiber reinforced concrete. *Eng. Fract. Mech.* **2000**, *65*, 235–245. [CrossRef]
26. Sangeetha, S.; Sakthieswaran, N.; Babu, O.G. Effect of steel fibre on fracture toughness of concrete. *Mater. Today Proc.* **2021**, *37*, 1036–1040. [CrossRef]
27. Sobuz, M.H.R.; Saha, A.; Anamika, J.F.; Houda, M.; Azab, M.; Akid, A.S.M.; Rana, M.J. Development of Self-Compacting Concrete Incorporating Rice Husk Ash with Waste Galvanized Copper Wire Fiber. *Buildings* **2022**, *12*, 1024. [CrossRef]
28. Siad, H.; Kamali-Bernard, S.; Mesbah, H.A.; Escadeillas, G.; Mouli, M.; Khelafi, H. Characterization of the degradation of self-compacting concretes in sodium sulfate environment: Influence of different mineral admixtures. *Constr. Build. Mater.* **2013**, *47*, 1188–1200. [CrossRef]
29. Sosa, I.; Tamayo, P.; Sainz-Aja, J.A.; Thomas, C.; Setién, J.; Polanco, J.A. Durability aspects in self-compacting siderurgical aggregate concrete. *J. Build. Eng.* **2021**, *39*, 102268. [CrossRef]
30. Hai, R.; Liu, P.; Yang, Y.; Liu, J. Mechanical properties of steel fiber reinforced fly ash self-compacting concrete. *J. Build. Mater.* **2021**, *24*, 87–92. (In Chinese) [CrossRef]
31. Ministry of Housing and Urban-Rural Development of People's Republic of China. *Technical Specification for Application of Self-Compacting Concrete: JGJ/T283*; China Building Industry Press: Beijing, China, 2012.
32. Ministry of Housing and Urban-Rural Development of People's Republic of China. *Standard for Test Methods of Long-Term Performance and Durability of Ordinary Concrete: GB/T50082*; China Building Industry Press: Beijing, China, 2009.
33. Emad, A.H.; Alwesabi, B.H.; Bakar, A.; Ibrahim, M.H.; Alshaikh; Zeyad, A.M.; Altheeb, A.; Alghamdi, H. Experimental investigation on fracture characteristics of plain and rubberized concrete containing hybrid steel-polypropylene fiber. *Structures* **2021**, *33*, 4421–4432. [CrossRef]
34. *ASTM E647-11*; Standard Test Method for Measurement of Fatigue Crack Growth Rates. ASTM: West Conshohocken, PA, USA, 2011.
35. Gao, D.; Zhang, T. Fraction characteristcs of steel fiber reinforced high strength concrete under three-point bending. *J. Chin. Ceram. Soc.* **2007**, *35*, 1630–1635. (In Chinese) [CrossRef]

36. Zeng, H.; Li, Y.; Zhang, J.; Chong, P.; Zhang, K. Effect of limestone powder and fly ash on the pH evolution coefficient of concrete in a sulfate-freeze-thaw environment. *J. Mater. Res. Technol.* **2022**, *16*, 1889–1903. [CrossRef]
37. Li, G.; Gao, X. Effects of secondary water curing on the long-term strength and durability of concrete after steam-autoclave curing. *J. Southeast Univ. Engl. Ed.* **2018**, *34*, 488–494. [CrossRef]
38. Zhao, Y.; Gao, J.; Qi, B.; Liu, C. Effect of flexural loading on degradation progress of recycled aggregate concrete subjected to sulfate attack and wetting-drying cycles. *J. Southeast Univ. Engl. Ed.* **2019**, *35*, 85–90. [CrossRef]
39. Köksal, F.; Şahin, Y.; Gencel, O.; Yiğit, I. Fracture energy-based optimisation of steel fibre reinforced concretes. *Eng. Fract. Mech.* **2013**, *107*, 29–37. [CrossRef]
40. Wang, K.; Guo, J.; Yang, L.; Zhang, P.; Xu, H. Multiphysical damage characteristics of concrete exposed to external sulfate attack: Elucidating effect of drying-wetting cycles. *Constr. Build. Mater.* **2022**, *329*, 127143. [CrossRef]
41. Chen, H. *Experimental Study on the Fracture Behavior of Concrete under Sulfate Corrosion under Dry-Wet Cycles*; Zhengzhou University: Zhengzhou, China, 2016. (In Chinese)
42. Sharma, R.; Khan, R.A. Sulfate resistance of self-compacting concrete incorporating copper slag as fine aggregates with mineral admixtures. *Constr. Build. Mater.* **2021**, *287*, 122985. [CrossRef]
43. Song, Y.; Zhou, S.; Wang, Z. Mechanism of Thaumasite Formation in Concrete. *J. Wuhan Univ. Technol.-Mater. Sci. Ed.* **2017**, *32*, 893–897. [CrossRef]